

# VectorMapNet: End-to-end Vectorized HD Map Learning

Yicheng Liu<sup>1</sup>   Yue Wang<sup>2</sup>   Yilun Wang<sup>3</sup>   Hang Zhao<sup>1 \*</sup>  
<sup>1</sup>Tsinghua University   <sup>2</sup>MIT   <sup>3</sup>Li Auto

**Abstract:** Autonomous driving systems require a good understanding of surrounding environments, including moving obstacles and static High-Definition (HD) semantic maps. Existing methods approach the semantic map problem by offline manual annotations, which suffer from serious scalability issues. More recent learning-based methods produce dense rasterized segmentation predictions which do not include instance information of individual map elements and require heuristic post-processing that involves many hand-designed components, to obtain vectorized maps. To that end, we introduce an end-to-end vectorized HD map learning pipeline, termed VectorMapNet. VectorMapNet takes onboard sensor observations and predicts a sparse set of polylines primitives in the bird’s-eye view to model the geometry of HD maps. Based on this pipeline, our method can explicitly model the spatial relation between map elements and generate vectorized maps that are friendly for downstream autonomous driving tasks without the need for post-processing. In our experiments, VectorMapNet achieves strong HD map learning performance on nuScenes dataset, surpassing previous state-of-the-art methods by 14.2 mAP. Qualitatively, we also show that VectorMapNet is capable of generating comprehensive maps and capturing more fine-grained details of road geometry. To the best of our knowledge, VectorMapNet is the first work designed toward end-to-end vectorized HD map learning problems.

**Keywords:** Autonomous Driving, Map Learning, Transformer

## 1 Introduction

Autonomous driving system requires an understanding of map elements on the road, including lanes, pedestrian crossing, and traffic signs, to navigate the world and plan ahead. Such map elements are typically provided by pre-annotated High-Definition (HD) semantic maps in existing pipelines [1]. These methods suffer from serious scalability issues as human labors are heavily involved in annotating HD maps. Recent works [2, 3, 4] explore the problem of online HD semantic map learning, where the goal is to use onboard sensors (*e.g.* LiDARs and cameras) to estimate map elements on-the-fly.

Most recent methods [4, 5, 3, 6] consider HD semantic map learning as a semantic segmentation problem in bird’s-eye view (BEV), which rasterizes map elements into pixels and assigns each pixel with a class label. This setting makes it straightforward to leverage fully convolutional networks and achieves promising results. However, rasterized maps are not an ideal map representation for autonomous driving for three reasons. First, rasterized maps lack instance information which is necessary to distinguish map elements with the same class label but different semantics, *e.g.* left lane markings and right lane markings. Second, map elements need a compact representation (*e.g.* vectorized representation) to ensure that they can be used for downstream tasks like prediction and planning. Nevertheless, it is hard to enforce consistency across pixels within the predicted rasterized map, *e.g.* nearby lane pixels might have contradicted semantics or geometries. Third, the rasterized map is incompatible with most autonomous driving systems as these systems commonly employ instance-level vectorized representation for HD maps. To predict vectorized representations, HDMapNet [2] generates semantic, instance, and directional maps and vectorizes these three maps with a hand-designed post-processing algorithm.

---

\*Correspond to hangzhao@mail.tsinghua.edu.cn

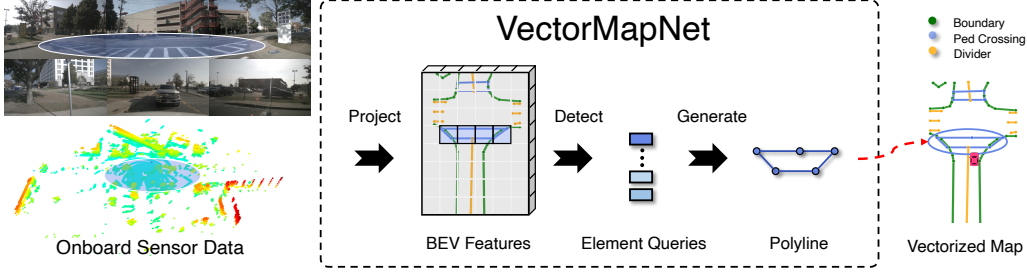


Figure 1: An overview of VectorMapNet. BEV features encode sensor data in the same coordinate as map elements. VectorMapNet detects the locations of map elements from BEV features by leveraging element queries. The vectorized HD map is built upon a sparse set of polylines that are generated from the detection results.

However, HDMapNet still relies on the rasterized map predictions, and its heuristic post-processing step complicates the pipeline and restricts the model’s scalability and performance. In this paper, we propose an end-to-end vectorized HD map learning model called VectorMapNet, which does not generate a dense set of semantic pixels. Instead, we represent map elements as a set of polylines that are easily linked to downstream tasks (*e.g.* motion forecasting [7]). Therefore, the map learning problem boils down to predicting a sparse set of polylines from sensor observations. We leverage state-of-the-art set prediction and sequence generation methods to generate map elements in three steps: First, VectorMapNet aggregates features generated from different modalities (*e.g.* camera images and LiDAR) into a common BEV feature space. Then, learnable queries detect map elements’ location and build a coarse map layout based on BEV features. Finally, given the coarse layout, we generate the polyline of each map element. We provide an overview of our idea in Figure 1 and discuss our motivation behind the problem in Section 2.

Our experiments show that VectorMapNet achieves dominant performance on the public nuScenes dataset, outperforming HDMapNet and other baselines by at least 14.2 mAP. Qualitatively, We find that VectorMapNet can build a more comprehensive map compared to previous works and is capable of capturing fine details, *e.g.* jagged boundaries, which are hard to capture by previous methods.

To summarize, the contributions of the paper are as follows:

- VectorMapNet is an end-to-end HD semantic map learning method. Unlike previous works, it uses polylines to represent map elements and directly predicts vectorized outputs from sensor observations without requiring map rasterization or post-processing.
- Jointly modeling the topological relations between map elements and the geometry of each map element is challenging. We leverage polylines as primitives to model complex map elements and mitigate this difficulty by decoupling this joint module into two parts: a map element detector and a polyline generator.
- VectorMapNet achieves state-of-the-art HD semantic map learning performance on nuScenes dataset. Both quantitative and qualitative results confirm our design choices.

## 2 VectorMapNet

**Problem formulation.** Similar to HDMapNet [2], our task is to model map elements in the urban environments in a vectorized form using data from onboard sensors, *e.g.* RGB cameras and/or LiDARs. These map elements include but are not limited to road boundaries, lane dividers, and pedestrian crossings, which are critical for autonomous driving.

As described above, we formulate this task as a sparse set prediction problem. Specifically, we represent a map  $\mathcal{M}$  by a sparse set of compact vectorized primitives, and the problem is to learn a model that extracts information from sensors to predict a set of vectorized primitives to represent the semantic map. For the vectorized representations, we opt to use  $N$  polylines  $\mathcal{V}^{\text{poly}} = \{V_1^{\text{poly}}, \dots, V_N^{\text{poly}}\}$  to represent map elements in the environment. Each polyline  $V^{\text{poly}} = \{v_i \in \mathbb{R}^2 | i = 1, \dots, N_v\}$  is a collection of  $N_v$  ordered vertices  $v_i$ . This setting enables us to model the spatial and topological relations between the map elements and emphasizes the instance characteristic of map elements as well.

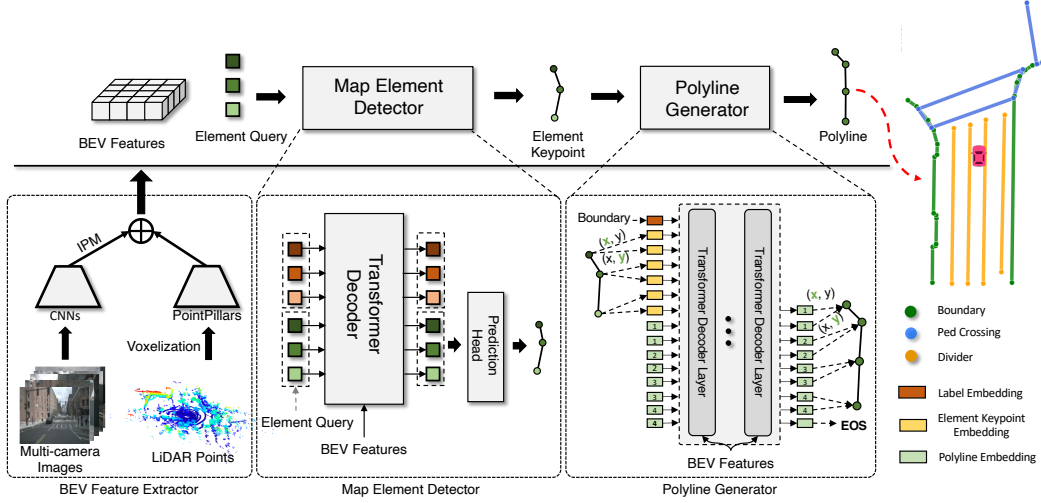


Figure 2: The network architecture of VectorMapNet. The top row is the pipeline of VectorMapNet generating polylines from raw sensor inputs. The bottom row illustrates detailed structures and inference procedures of three primary components of VectorMapNet: BEV feature extractor, map element detector, and polyline generator.

Moreover, using polylines to represent map elements has three main advantages: (1) HD maps are typically composed of a mixture of different geometries, such as points, lines, curves, and polygons. Polyline is a flexible primitive that can represent these geometries effectively. (2) The order of polyline vertices is a natural way to encode the direction information of map elements, which is vital for vehicle planning. (3) The polyline representation has been widely employed by downstream autonomous driving modules, such as motion forecasting [7].

**Overviews.** To solve this problem, first we need to map sensor data from sensor-view to a canonical BEV representation  $\mathcal{F}_{\text{BEV}}$ . Then the remaining task is to model polylines based on  $\mathcal{F}_{\text{BEV}}$ . However, the structural patterns and the location of map elements have a broad diversity, and jointly learning them can be challenging. Thus, we decouple the modeling task into two parts: (1) A scene-level element detection task that locates and classifies all map elements by predicting element keypoints  $\mathcal{A} = \{a_i \in \mathbb{R}^{k \times 2} | i = 1, \dots, N\}$  and their class labels  $\mathcal{L} = \{l_i \in \mathbb{Z} | i = 1, \dots, N\}$ ; (2) A object-level sequence generation task that produces a polyline vertices sequence for each detected map element  $(a_i, l_i)$ . The definitions of element keypoint representation  $\mathcal{A}$  are described in Section 2.2.

Correspondingly, VectorMapNet employs three modules to model these three tasks (see Figure 2). It first uses a BEV feature extractor to elevate sensor observation to BEV spaces, and then passes the BEV features to a map element detector from which we get element keypoints  $\mathcal{A}$  and class labels  $\mathcal{L}$ . Finally, a polyline generator generates the polyline sequence to construct the HD map conditioned on element keypoints, class labels, and BEV features.

## 2.1 BEV Feature Extractor

The BEV feature extractor projects information from various modality inputs into a unified feature space and aggregates these features into a canonical representation termed BEV features  $\mathcal{F}_{\text{BEV}}$ . We consider two common modalities: surrounding camera images  $\mathcal{I}$  and LiDAR points  $\mathcal{P}$ .

**Camera branch.** For image data  $\mathcal{I}$ , we use a shared CNN backbone to obtain each camera’s image feature in camera space, then use Inverse Perspective Mapping (IPM) technique to transform these features into BEV space. Since the depth information is missing in camera images, we follow one common approach that assumes the ground is mostly planar and transforms the images to BEV with a simple homography. Without knowing the exact height of the ground plane, this homography is not an accurate transformation. To alleviate this issue, we transform the image features into four BEV planes with different heights  $(-1m, 0m, 1m, 2m)$ . The camera BEV features  $\mathcal{F}_{\text{BEV}}^{\mathcal{I}} \in \mathbb{R}^{W \times H \times C_1}$  are the concatenation of these feature maps.

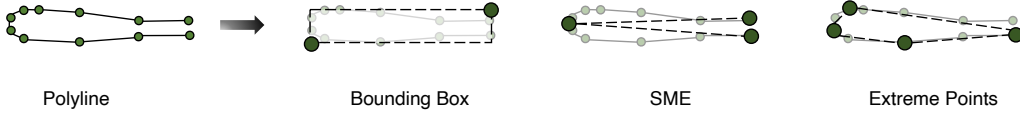


Figure 3: Keypoint representations of map elements. Three different keypoint representations are proposed here: Bounding Box, SME, and Extreme Points.

**LiDAR branch.** For LiDAR data  $\mathcal{P}$ , we use a variant of PointPillars [8] with dynamic voxelization [9], which divides the 3D space into multiple pillars and uses pillar-wise point clouds to learn pillar-wise feature maps. This feature map in BEV is denoted as  $\mathcal{F}_{\text{BEV}}^P \in \mathbb{R}^{W \times H \times C_2}$ . For sensor fusion, we obtain the BEV features  $\mathcal{F}_{\text{BEV}} \in \mathbb{R}^{W \times H \times (C_1 + C_2)}$  by concatenating  $\mathcal{F}_{\text{BEV}}^T$  and  $\mathcal{F}_{\text{BEV}}^P$ , and then process the concatenated result through a two-layer convolutional network.

An overview of the BEV feature extractor is shown at the bottom-left of Figure 2. Since the following modules of VectorMapNet are variants of transformer, we flatten the BEV features  $\mathcal{F}_{\text{BEV}}$  to a sequence  $\mathcal{F}_{\text{BEV}}^f \in \mathbb{R}^{W \times H \times (C_1 + C_2)}$ . We then add fixed positional encoding to the sequence to encode spatial information and connect the flattened BEV features  $\mathcal{F}_{\text{BEV}}^f$  with map elements  $\mathcal{M}$ .

## 2.2 Map Element Detector

After projecting onboard sensor data to BEV features, the goal of map element detector is to infer keypoints of each map element from the BEV features  $\mathcal{F}_{\text{BEV}}$ . We leverage a variant of transformer-based set prediction detector [10] to achieve this goal. This detector represents map elements' locations and categories by predicting their element keypoints  $\mathcal{A}$  and class labels  $\mathcal{L}$ . The geometric relations between these elements are modeled by the attention module in the detector. Moreover, the detector is trained with bipartite matching loss, enabling VectorMapNet to avoid post-processing steps like non-maximum suppression (NMS).

**Element queries.** The inputs of the detector are learnable element queries  $\{q_i^{\text{elem}} \in \mathbb{R}^{k \times d} | i = 1, \dots, N_{\text{max}}\}$ , where  $d$  is the hidden embedding size, and the  $i$ -th element query  $q_i^{\text{elem}}$  is composed of  $k$  keypoints:  $q_i^{\text{elem}} = \{q_{i,j}^{\text{kp}} \in \mathbb{R}^d | j = 1, \dots, k\}$ .

**Architecture.** The basic architecture of map element detector includes a transformer decoder [11] and a prediction head, which is similar to DETR-like models [12, 13, 14] (see the bottom-middle of Figure 2). We flatten element queries into a sequence  $\{q_i^{\text{kp}} \in \mathbb{R}^d | i = 1, \dots, N_{\text{max}} \cdot k\}$  to meet the decoder input requirement. Similar to DETR, the decoder transforms the flattened element queries using multi-headed self- and cross-attention mechanisms. The cross attention module of the detector takes BEV feature sequence as its keys and values. Moreover, we use the deformable attention module [12] as the decoder's cross attention module, where each query in the decoder has a 2D location in BEV features, to build a one-to-one correspondence between predicted keypoints and BEV space and accelerate training convergence [15].

The prediction head decodes element queries processed by the decoder to element keypoints and their class labels with two branches: a regression branch (denoted as  $PH_{\text{reg}}$ ) and a classification branch (denoted as  $PH_{\text{cls}}$ ). For each map element, the regression branch predicts the coordinates of each keypoint  $a_{i,j}$  from keypoint embedding  $q_{i,j}^{\text{kp}}$  via a shared multi-layer perceptron  $\{a_{i,j} = PH_{\text{reg}}(q_{i,j}^{\text{kp}}) | i = 1 \dots N_{\text{max}}, j = 1 \dots k\}$ . The class label of each map element  $l_i$  is predicted by the classification branch from the concatenation of these keypoint embeddings for individual map element via a linear projection layer:  $l_i = PH_{\text{cls}}([q_{i,1}^{\text{kp}}, \dots, q_{i,k}^{\text{kp}}])$ .

**Keypoint representation of map elements.** We use keypoints to represent the location and outline of map elements in a compact way. Since there is no straightforward keypoint design for polylines, we propose three simple representations as shown in Figure 3: Bounding box, which is the smallest box enclosing a polyline, and its keypoints are defined as the top-right and bottom-left points of the box; Start-Middle-End (SME), which consists of the start, middle, and end point of a polyline; Extreme points, which are the left-most, right-most, top-most, and bottom-most points of a polyline. An ablation study is conducted to evaluate their performance in supplementary material.

**Keypoint embeddings.** Each keypoint  $q^{\text{kp}}$  in the map element detector has two learnable embeddings for the attention modules to identify the difference between keypoints. The first embedding is keypoint position embedding  $\{e_j^{\text{kp}} \in \mathbb{R}^d | j = 1, \dots, k\}$ , indicating which position the keypoint belongs to in a keypoint. The second embedding  $\{e_i^{\text{p}} \in \mathbb{R}^d | i = 1, \dots, N_{\text{max}}\}$  encodes which map element the keypoint belongs to. The keypoint embedding is the addition of these two embeddings  $e_i^{\text{p}} + e_j^{\text{kp}}$ .

### 2.3 Polyline Generator

The goal of polyline generator is to generate the detailed geometry of map elements. Specifically, polyline generator models a distribution  $p(V_i^{\text{poly}} | a_i, l_i, \mathcal{F}_{\text{BEV}})$  over each polyline, conditioned on the initial layout (*i.e.*, element keypoints and class labels) and BEV features, and VectorMapNet use this distribution to infer the vertices of polylines. For each polyline  $V_i^{\text{poly}} = \{v_{i,n} \in \mathbb{R}^2 | n = 1, \dots, N_v\}$ , we obtain flattened polyline sequence  $\{v_{i,n}^f \in \mathbb{R} | n = 1, \dots, 2N_v\}$  by concatenating coordinates values of polyline vertices. An additional *End of Sequence* token  $EOS$  is added at the end of each sequence. To estimate this distribution, we decompose the joint distribution over  $V_i^{\text{poly}}$  as a product of a series of conditional vertex coordinate distributions:

$$p(V_i^{\text{poly}} | a_i, l_i, \mathcal{F}_{\text{BEV}}; \theta) = \prod_{t=1}^{2N_v} p(v_{i,t}^f | v_{i,<t}^f, a_i, l_i, \mathcal{F}_{\text{BEV}}; \theta). \quad (1)$$

We model this distribution using an autoregressive network that outputs the parameters of a predictive distribution at each step for the next vertex coordinate. This predictive distribution is defined over vertex coordinate values and end of sequence token  $EOS$ . Polyline generator is trained to maximize the log-probability of the observed polylines with respect to the model parameters  $\theta$  and  $\mathcal{F}_{\text{BEV}}$ .

**Architecture.** We use a transformer decoder to model the positions of vertices (see the bottom-right of Figure 2). The generator takes the polyline keypoints' coordinate values and its class label as the initial inputs of the transformer decoder. The queries of the transformer decoder integrate BEV features with cross attention modules. These queries are then decoded to vertex coordinate values iteratively via a linear projection layer. We use an improved transformer variant with layer normalization inside the residual path [16, 17], which improves the efficiency of training processing.

**Vertices as discrete variables.** Using discrete distribution to model the vertices of polyline has the advantage of representing arbitrary vertex location distributions in the maps. For instance, categorical distribution can easily represent various shapes, such as multi-modal, skewed, peaked, or long-tailed, that are commonly seen in our task. Therefore, we quantize the polyline vertices' coordinate values into discrete tokens and model each token with a categorical distribution. Specifically, we quantize the map space into bins and merge the vertex values that fell into the same bin. We also conduct an ablation study in Section 3.3 to investigate other modeling choices.

**Polyline embeddings.** Following PolyGen [18], we use three learned embeddings to represent each token's properties: *Coordinate embedding*, indicating whether the token represents  $x$  or  $y$  coordinate; *Position embedding*, representing which vertex the token belongs to; *Value embedding*, expressing the token's quantized coordinate value.

## 3 Experiments

We experiment on nuScenes [19] dataset and use average precision as the evaluation metric. The details of model, metric and dataset settings are in supplementary material.

### 3.1 Comparison with baselines

We choose two closely related models as our baselines, HDMapNet [2] and STSU [20]. For HDMapNet, we directly take its vectorized results. STSU uses a transformer module to detect the moving objects and centerline segments. It uses an association head to piece the segments together as the road graph. In order to adapt STSU to our task, we use a two-layer multi-layer perceptron to predict lane segments and only keep its object branch and polyline branch. We report the average precision that uses Chamfer distance as the threshold to determine the positive matches with ground truth.  $\{0.5, 1.0, 1.5\}$  are the predefined thresholds of Chamfer distance.

As shown in Table 1, VectorMapNet outperforms HDMapNet by a large margin under all settings (+17.9 mAP in Camera, +9.9 mAP in LiDAR, and +11.7 mAP in Fusion). Compared to camera-only



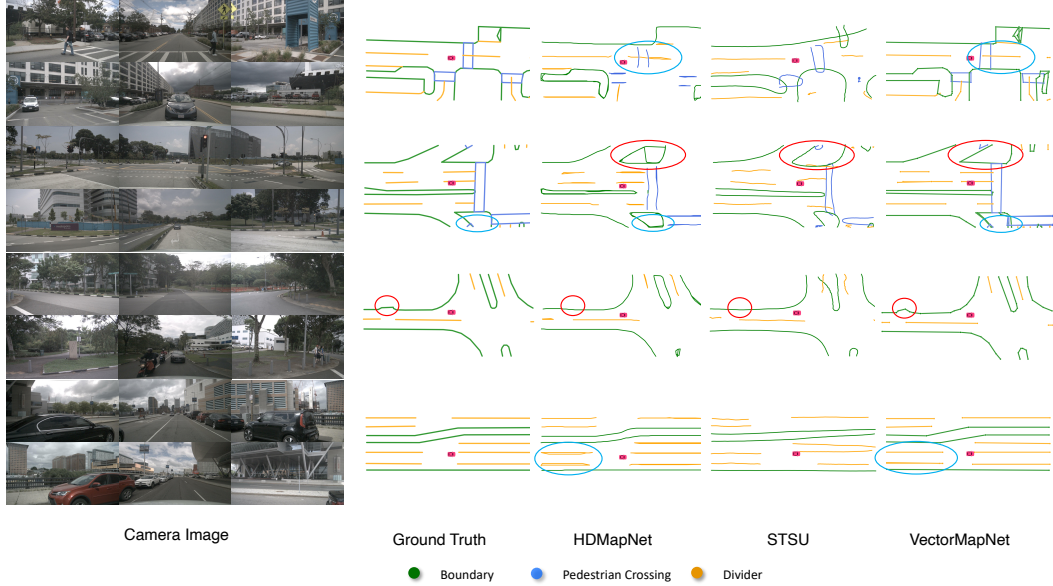


Figure 4: Qualitative results generated by VectorMapNet and baselines. We use camera images for comparisons. The areas enclosed by red and blue ellipses show that VectorMapNet can preserve sharp corners, and polyline representations prevent VectorMapNet from generating ambiguous self-looping results.

Table 1: Comparison with baselines. AP & mAP: higher is better. STSU, HDMaNet (Camera), and VectorMapNet (Camera) take surrounding camera images as inputs. HDMaNet (LiDAR) and VectorMapNet (LiDAR) take LiDAR points as inputs. VectorMapNet (Fusion) and HDMaNet (Fusion) take both surrounding camera images and LiDAR points as inputs.

Methods	$AP_{ped}$	$AP_{divider}$	$AP_{boundary}$	mAP
STSU[20]	7.0	11.6	16.5	11.7
HDMaNet (Camera) [2]	14.4	21.7	33.0	23.0
HDMaNet (LiDAR) [2]	10.4	24.1	37.9	24.1
HDMaNet (Fusion) [2]	16.3	29.6	46.7	31.0
VectorMapNet (Camera)	36.1	47.3	39.3	40.9
VectorMapNet (LiDAR)	25.7	37.6	38.6	34.0
VectorMapNet (Fusion)	<b>37.6</b>	<b>50.5</b>	<b>47.5</b>	<b>45.2</b>

and LiDAR-only, sensor fusion introduces +4.3 mAP improvement and +11.2 mAP improvement, respectively. STSU is -29.2 mAP lower than VectorMapNet. Since STSU treats all map elements as a set of fixed-size segments, we hypothesize that ignoring the structure of map elements hurts the performance significantly.

### 3.2 Qualitative Analysis

**Benefits of using polylines as primitives.** From visualizations, we find that using polylines as primitives has brought us two benefits compared with baselines: First, polylines alleviate the difficulty of encoding the detailed context of map elements. VectorMapNet preserves most of the detailed context (*e.g.* the corners of boundaries). The models that use dense lane segments and pixels are hard to learn these geometric details, as these representations require accurately classifying all their elements to preserve the geometric structure. Otherwise, the details will be changed (see the red ellipses in Figure 4). Second, polyline representations prevent VectorMapNet from generating ambiguous results, as it can consistently encode direction information. Models without this consistency constrain are prone to generating loop curves that falsely represent one-way lane dividers with two directions and connect two lanes with conflict direction (see the blue ellipses in Figure 4). These ambiguities hinder safe autonomous driving. To summarize, the polyline is a desired primitive for map learning, as it can reflect the real-world road layout and implicitly encode traffic rules.

**Benefits of modeling topological relations between map elements.** Every map element is an indispensable part of the traffic rule that restrains every traffic participant. VectorMapNet uses a self-attention mechanism to model the topological relations between map elements' location in the

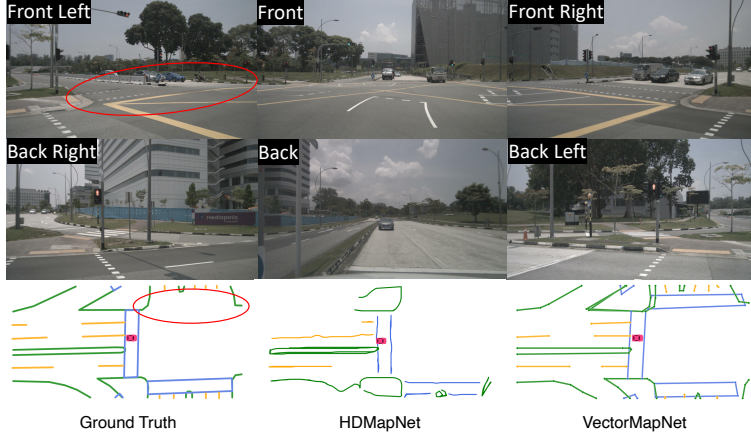


Figure 5: An example of VectorMapNet detects unlabeled map elements. Red ellipses indicate a pedestrian crossing that is missing in ground truth annotations. Only the VectorMapNet detects it correctly. All the predictions are generated from camera images.

map element detector and then generates the details. According to experiment results, we find that VectorMapNet can capture most of the map elements in the map, including the small elements located at the edges. Furthermore, Figure 5 shows that VectorMapNet can find the map elements that are not annotated in the HD map provided by the dataset. This observation shows the potential of the proposed learning-based method to replace the traditional HD map human annotation pipeline.

### 3.3 Ablation Studies

In this section, we explore how the sampling strategies of polyline vertices, modeling of polylines, and keypoint representations influence the model performance. We report two average precisions, Chamfer AP and Fréchet AP. The threshold of Fréchet distance APs is chosen as  $5m$ , and the calculation of Chamfer distance APs are the same as in Section 3.1.

Table 2: Ablation study of curves sampling strategies.

Vertex Sampling Method	Fréchet Distance				Chamfer Distance			
	$AP_{ped}$	$AP_{divider}$	$AP_{boundary}$	mAP	$AP_{ped}$	$AP_{divider}$	$AP_{boundary}$	mAP
curvature-based	47.0	47.4	56.9	50.4	27.6	34.4	35.4	32.5
fixed interval	26.0	23.6	37.1	28.9	14.6	17.6	18.7	17.0

**Curve sampling strategies.** There are two basic ways to sample curves to polylines. The first is based on the nuScenes setting [19], which samples vertices at the position where the curvature changes are beyond a certain threshold. The second is sampling the vertices at fixed intervals ( $1m$ ). The results are shown in Table 2. The curvature-based sampling outperforms fixed-sampling by a large margin and achieves a lead of 21.5 Fréchet mAP and 15.5 Chamfer mAP. We hypothesize that the fixed-sampling method involves many vertices that have a negligible contribution to the geometry. These redundant vertices hurt the generator’s learning by averaging out the weight of essential vertices (*e.g.* the vertices at the corner of a polyline) in the learning process.

Table 3: Ablation study of polyline modeling methods.

Modeling Method	Fréchet Distance				Chamfer Distance			
	$AP_{ped}$	$AP_{divider}$	$AP_{boundary}$	mAP	$AP_{ped}$	$AP_{divider}$	$AP_{boundary}$	mAP
discrete	47.0	47.4	56.9	50.4	27.6	34.4	35.4	32.5
continuous	38.0	41.6	46.1	41.9	26.5	28.1	30.1	26.5

**Polyline modeling methods.** We investigate both discrete and continuous ways of modeling the generated polylines. The discrete version of polyline generator is described in Section 2.3. With the same model structure, we follow SketchRNN [21] by using a mixture of Gaussian distribution to model the vertices of polylines as a continuous variable. The comparison is shown in Table 3. We find that using discrete rather than continuous embeddings for vertex coordinates results in a considerable gain in performance, with Chamfer mAP increasing from 18.2 to 32.5 and the Fréchet

mAP increasing from 26.8 to 50.4. These improvements suggest that the non-local characteristic of categorical distribution helps our model capture the various vertex coordinate distribution.

## 4 Related Works

**Semantic map learning.** Annotating the semantic information of surrounding environment to a map is an area of growing concern. With the help of deep learning, semantic map learning is formulated as a semantic segmentation problem [22] and solved by using aerial images [23], LiDAR points [5] and HD panorama [24]. The crowdsourcing tags [25] are used to improve the performance of fine-grained segmentation. Instead of using offline data, some researchers focus on understanding BEV semantics from onboard camera images [26, 27], and video [28]. Only using onboard sensors as model input is particularly challenging as the inputs and target map lie in different coordinate frames. Recently, several cross-view learning approaches [3, 29, 2, 6] leverage the geometric structure of scenes to mitigate the mismatch between sensor and BEV space. Beyond the pixel-level semantic map, our work extracts a consistent vectorized map around vehicles from surrounding cameras or LiDARs, which is friendly for downstream tasks like motion prediction [7, 30, 31].

**Lane detection.** Lane detection aims to separate lane segments from road scenes precisely. Most lane detection algorithms [32, 33] use a pixel-level segmentation technique combined with sophisticated post-processing. Another line of work leverages the predefined proposal to achieve high accuracy and fast inference speed. These methods typically involve handcrafted elements such as vanishing points [34], polynomial curves [35], line segments [36], and Bézier curves [37] to model proposals. In addition to using perspective view cameras as inputs, the authors of [38] and [39] extract lane segments from overhead highway cameras and LiDAR imagery with a recurrent neural network. Instead of discovering the road’s topology via boundaries detection, STSU [20] constructs lane graphs by using the centerline segment encoded by Bézier curve as primitive. To model complex geometries in the urban environment, we leverage polylines to represent the whole map elements in perceptual scope instead of handcrafted elements. Using polylines as primitive allows our method to model maps without complicated geometric assumptions and express map elements with arbitrary shapes.

**Geometric data modeling.** Another line of work closely related to VectorMapNet is geometric data generation. These methods typically treat geometric elements as a sequence, such as primitive parts of furniture [40, 41], states of sketch strokes [21], and vertices of  $n$ -gon mesh [18], and generate these sequences by leveraging autoregressive models. Since the directly modeling sequence is challenging for long-range centerline maps, HDMapGen [42] views the map as a two-level hierarchy. It produces a global and local graph separately with a hierarchical graph RNN. Instead of treating geometric elements as a sequence generation problem, LETR [43] models line segment as a detection problem and tackle it with a query-based detector. Unlike the above approaches that focus on single-level geometric modelings, such as scene level (*e.g.* line segments in an image) or object-level (*e.g.* furniture), VectorMapNet is designed to address both the scene level and object level geometric modeling. Specifically, VectorMapNet constructs a map by modeling the global relationship between map elements in the scene and the local geometric details inside each element.

## 5 Conclusions

We present VectorMapNet, an end-to-end model to tackle HD semantic map learning problems. Unlike existing works, VectorMapNet uses polylines as primitives to represent vectorized HD map elements. To learn these polylines, we decompose the learning problem into a detection and a generation problem. Our experiments show that VectorMapNet can generate coherent and complex geometries for urban map elements benefiting from the polyline primitives. We believe that this novel way to learn HD maps provides a new perspective on the HD semantic map learning problem.

**Limitations.** Although our method can generate coherent and complex geometries in a single frame, temporally consistent predictions are not guaranteed. How to effectively encode temporal information for vectorized HD map prediction is challenging, which we left as future work.

## Acknowledgments

We would like to thank Qi Li, Tianyuan Zhang, and Tianyuan Yuan for their help on various baselines. We also benefited from proofreading by Ziyuan Huang and Bowen Li.



## References

- [1] G. Rong, B. H. Shin, H. Tabatabaee, Q. Lu, S. Lemke, M. Možeiko, E. Boise, G. Uhm, M. Gerow, S. Mehta, et al. Lgsvl simulator: A high fidelity simulator for autonomous driving. *arXiv preprint arXiv:2005.03778*, 2020.
- [2] Q. Li, Y. Wang, Y. Wang, and H. Zhao. Hdmapnet: A local semantic map learning and evaluation framework. *arXiv preprint arXiv:2107.06307*, 2021.
- [3] J. Phillion and S. Fidler. Lift, splat, shoot: Encoding images from arbitrary camera rigs by implicitly unprojecting to 3d. In *European Conference on Computer Vision*, pages 194–210. Springer, 2020.
- [4] T. Roddick and R. Cipolla. Predicting semantic map representations from images using pyramid occupancy networks. In *Proceedings of the IEEE/CVF Conference on Computer Vision and Pattern Recognition*, pages 11138–11147, 2020.
- [5] B. Yang, M. Liang, and R. Urtasun. Hdnet: Exploiting hd maps for 3d object detection. In *Conference on Robot Learning*, pages 146–155. PMLR, 2018.
- [6] B. Zhou and P. Krähenbühl. Cross-view transformers for real-time map-view semantic segmentation. *arXiv preprint arXiv:2205.02833*, 2022.
- [7] J. Gao, C. Sun, H. Zhao, Y. Shen, D. Anguelov, C. Li, and C. Schmid. Vectornet: Encoding hd maps and agent dynamics from vectorized representation. In *Proceedings of the IEEE/CVF Conference on Computer Vision and Pattern Recognition*, pages 11525–11533, 2020.
- [8] A. H. Lang, S. Vora, H. Caesar, L. Zhou, J. Yang, and O. Beijbom. Pointpillars: Fast encoders for object detection from point clouds. In *Proceedings of the IEEE/CVF Conference on Computer Vision and Pattern Recognition*, pages 12697–12705, 2019.
- [9] Y. Zhou, P. Sun, Y. Zhang, D. Anguelov, J. Gao, T. Ouyang, J. Guo, J. Ngiam, and V. Vasudevan. End-to-end multi-view fusion for 3d object detection in lidar point clouds. In *Conference on Robot Learning*, pages 923–932. PMLR, 2020.
- [10] N. Carion, F. Massa, G. Synnaeve, N. Usunier, A. Kirillov, and S. Zagoruyko. End-to-end object detection with transformers. In *European conference on computer vision*, pages 213–229. Springer, 2020.
- [11] A. Vaswani, N. Shazeer, N. Parmar, J. Uszkoreit, L. Jones, A. N. Gomez, Ł. Kaiser, and I. Polosukhin. Attention is all you need. *Advances in neural information processing systems*, 30, 2017.
- [12] X. Zhu, W. Su, L. Lu, B. Li, X. Wang, and J. Dai. Deformable detr: Deformable transformers for end-to-end object detection. *arXiv preprint arXiv:2010.04159*, 2020.
- [13] Y. Wang, V. C. Guizilini, T. Zhang, Y. Wang, H. Zhao, and J. Solomon. Detr3d: 3d object detection from multi-view images via 3d-to-2d queries. In *Conference on Robot Learning*, pages 180–191. PMLR, 2022.
- [14] X. Chen, T. Zhang, Y. Wang, Y. Wang, and H. Zhao. Futr3d: A unified sensor fusion framework for 3d detection. *arXiv preprint arXiv:2203.10642*, 2022.
- [15] F. Li, H. Zhang, S. Liu, J. Guo, L. M. Ni, and L. Zhang. Dn-detr: Accelerate detr training by introducing query denoising. *arXiv preprint arXiv:2203.01305*, 2022.
- [16] R. Child, S. Gray, A. Radford, and I. Sutskever. Generating long sequences with sparse transformers. *arXiv preprint arXiv:1904.10509*, 2019.
- [17] N. Parmar, A. Vaswani, J. Uszkoreit, L. Kaiser, N. Shazeer, A. Ku, and D. Tran. Image transformer. In *International Conference on Machine Learning*, pages 4055–4064. PMLR, 2018.

- [18] C. Nash, Y. Ganin, S. A. Eslami, and P. Battaglia. Polygen: An autoregressive generative model of 3d meshes. In *International Conference on Machine Learning*, pages 7220–7229. PMLR, 2020.
- [19] H. Caesar, V. Bankiti, A. H. Lang, S. Vora, V. E. Liong, Q. Xu, A. Krishnan, Y. Pan, G. Baldan, and O. Beijbom. nuscenes: A multimodal dataset for autonomous driving. In *Proceedings of the IEEE/CVF conference on computer vision and pattern recognition*, pages 11621–11631, 2020.
- [20] Y. B. Can, A. Liniger, D. P. Paudel, and L. Van Gool. Structured bird’s-eye-view traffic scene understanding from onboard images. In *Proceedings of the IEEE/CVF International Conference on Computer Vision*, pages 15661–15670, 2021.
- [21] D. Ha and D. Eck. A neural representation of sketch drawings. *arXiv preprint arXiv:1704.03477*, 2017.
- [22] G. Mattyus, S. Wang, S. Fidler, and R. Urtasun. Enhancing road maps by parsing aerial images around the world. In *Proceedings of the IEEE international conference on computer vision*, pages 1689–1697, 2015.
- [23] G. Mátyus, S. Wang, S. Fidler, and R. Urtasun. Hd maps: Fine-grained road segmentation by parsing ground and aerial images. In *Proceedings of the IEEE Conference on Computer Vision and Pattern Recognition*, pages 3611–3619, 2016.
- [24] S. Wang, M. Bai, G. Mattyus, H. Chu, W. Luo, B. Yang, J. Liang, J. Chaverie, S. Fidler, and R. Urtasun. Torontocity: Seeing the world with a million eyes. *arXiv preprint arXiv:1612.00423*, 2016.
- [25] S. Wang, S. Fidler, and R. Urtasun. Holistic 3d scene understanding from a single geo-tagged image. In *Proceedings of the IEEE Conference on Computer Vision and Pattern Recognition*, pages 3964–3972, 2015.
- [26] C. Lu, M. J. G. van de Molengraft, and G. Dubbelman. Monocular semantic occupancy grid mapping with convolutional variational encoder–decoder networks. *IEEE Robotics and Automation Letters*, 4(2):445–452, 2019.
- [27] W. Yang, Q. Li, W. Liu, Y. Yu, Y. Ma, S. He, and J. Pan. Projecting your view attentively: Monocular road scene layout estimation via cross-view transformation. In *Proceedings of the IEEE/CVF Conference on Computer Vision and Pattern Recognition*, pages 15536–15545, 2021.
- [28] Y. B. Can, A. Liniger, O. Unal, D. Paudel, and L. Van Gool. Understanding bird’s-eye view semantic hd-maps using an onboard monocular camera. *arXiv preprint arXiv:2012.03040*, 2020.
- [29] B. Pan, J. Sun, H. Y. T. Leung, A. Andonian, and B. Zhou. Cross-view semantic segmentation for sensing surroundings. *IEEE Robotics and Automation Letters*, 5(3):4867–4873, 2020.
- [30] H. Zhao, J. Gao, T. Lan, C. Sun, B. Sapp, B. Varadarajan, Y. Shen, Y. Shen, Y. Chai, C. Schmid, et al. Tnt: Target-driven trajectory prediction. *arXiv preprint arXiv:2008.08294*, 2020.
- [31] Y. Liu, J. Zhang, L. Fang, Q. Jiang, and B. Zhou. Multimodal motion prediction with stacked transformers. In *Proceedings of the IEEE/CVF Conference on Computer Vision and Pattern Recognition*, pages 7577–7586, 2021.
- [32] X. Pan, J. Shi, P. Luo, X. Wang, and X. Tang. Spatial as deep: Spatial cnn for traffic scene understanding. In *Proceedings of the AAAI Conference on Artificial Intelligence*, volume 32, 2018.
- [33] D. Neven, B. De Brabandere, S. Georgoulis, M. Proesmans, and L. Van Gool. Towards end-to-end lane detection: an instance segmentation approach. In *2018 IEEE intelligent vehicles symposium (IV)*, pages 286–291. IEEE, 2018.

- [34] S. Lee, J. Kim, J. Shin Yoon, S. Shin, O. Bailo, N. Kim, T.-H. Lee, H. Seok Hong, S.-H. Han, and I. So Kweon. Vpgnet: Vanishing point guided network for lane and road marking detection and recognition. In *Proceedings of the IEEE international conference on computer vision*, pages 1947–1955, 2017.
- [35] W. Van Gansbeke, B. De Brabandere, D. Neven, M. Proesmans, and L. Van Gool. End-to-end lane detection through differentiable least-squares fitting. In *Proceedings of the IEEE/CVF International Conference on Computer Vision Workshops*, pages 0–0, 2019.
- [36] X. Li, J. Li, X. Hu, and J. Yang. Line-cnn: End-to-end traffic line detection with line proposal unit. *IEEE Transactions on Intelligent Transportation Systems*, 21(1):248–258, 2019.
- [37] Z. Feng, S. Guo, X. Tan, K. Xu, M. Wang, and L. Ma. Rethinking efficient lane detection via curve modeling. *arXiv preprint arXiv:2203.02431*, 2022.
- [38] N. Homayounfar, W.-C. Ma, S. K. Lakshmikanth, and R. Urtasun. Hierarchical recurrent attention networks for structured online maps. In *Proceedings of the IEEE Conference on Computer Vision and Pattern Recognition*, pages 3417–3426, 2018.
- [39] J. Liang, N. Homayounfar, W.-C. Ma, S. Wang, and R. Urtasun. Convolutional recurrent network for road boundary extraction. In *Proceedings of the IEEE/CVF Conference on Computer Vision and Pattern Recognition*, pages 9512–9521, 2019.
- [40] J. Li, K. Xu, S. Chaudhuri, E. Yumer, H. Zhang, and L. Guibas. Grass: Generative recursive autoencoders for shape structures. *ACM Transactions on Graphics (TOG)*, 36(4):1–14, 2017.
- [41] K. Mo, P. Guerrero, L. Yi, H. Su, P. Wonka, N. Mitra, and L. J. Guibas. Structurennet: Hierarchical graph networks for 3d shape generation. *arXiv preprint arXiv:1908.00575*, 2019.
- [42] L. Mi, H. Zhao, C. Nash, X. Jin, J. Gao, C. Sun, C. Schmid, N. Shavit, Y. Chai, and D. Anguelov. Hdmapgen: A hierarchical graph generative model of high definition maps. In *Proceedings of the IEEE/CVF Conference on Computer Vision and Pattern Recognition*, pages 4227–4236, 2021.
- [43] Y. Xu, W. Xu, D. Cheung, and Z. Tu. Line segment detection using transformers without edges. In *Proceedings of the IEEE/CVF Conference on Computer Vision and Pattern Recognition*, pages 4257–4266, 2021.